

A Wireless Inductive-Capacitive Resonant Circuit Sensor Array for Force Monitoring

Andrew J. DeRouin, Brandon D. Pereles, Thadeus M. Sansom, Peng Zang, Keat Ghee Ong

Department of Biomedical Engineering, Michigan Technological University, Houghton, USA

Email: kgong@mtu.edu

Received July 11, 2013; revised August 11, 2013; accepted August 19, 2013

Copyright © 2013 Andrew J. DeRouin *et al.* This is an open access article distributed under the Creative Commons Attribution License, which permits unrestricted use, distribution, and reproduction in any medium, provided the original work is properly cited.

ABSTRACT

A wireless passive sensor array based on inductive-capacitive (LC) resonant circuits capable of simultaneously tracking two points of force loading is described. The sensor consisted of a planar spiral inductor connected to two capacitors forming a resonant circuit with two resonant frequencies. When a load was applied to one or both of the parallel plate capacitors, the distance between the plates of the capacitor was altered, thus shifting the observed resonant peaks. Testing illustrated that applied loading to a particular capacitor caused a significant shift in one of the resonant peaks and also a smaller shift in another resonant peak. This interdependence resulted from each capacitive element being connected to the same inductive spiral and was accounted for with a developed analysis algorithm. To validate the experimental observation, a circuit simulation was also generated to model the sensor behavior with changing force/displacement. The novelty of this system lies not only in its wireless passive nature, but also in the fact that a single LC sensor was fashioned to detect more than one point simultaneously.

Keywords: Force Sensors; RFID Tags; Sensor Array; Wireless Sensors

1. Introduction

Generally, wireless sensors consist of sensor components for taking local measurements placed at the areas of interest and a remotely located system to receive information wirelessly for processing and presentation [1-3]. Since these systems lack physical connections between the sensing components and the processing apparatus, they are highly versatile in terms of sensor deployment, and are thus ideal for wide area monitoring. Additionally, wireless sensors have the capacity to operate, depending on the particular method of data acquisition and transmission, in an active or passive mode. Active sensors are powered with an internal source whereas passive devices receive power remotely. While active wireless sensors can monitor a wide range of parameters encompassing a large region, they can also suffer from significant installation and maintenance costs and battery lifetime limitations [4]. Passive wireless sensors, on the other hand, have limited functionality compared to their active counterparts but are generally cheaper, easier to implement and last longer. There are many types of wireless passive sensors, and most of them are powered magnetically or electromagnetically. Examples of these sensors include magnetoelastic, inductive-capacitive, and surface acous-

tic sensors [5-9].

A wireless passive sensor, known as the inductive-capacitive (LC) sensor, was developed to monitor changing environmental conditions such as temperature, humidity and pressure [10]. This type of sensor altered its capacitance depending on the experienced environmental parameter, resulting in a shift in its resonant frequency. The change in resonant frequency was remotely captured with a coil antenna by monitoring its impedance change [10]. Unfortunately, the limitation of the existing LC sensors is their inability to monitor multiple parameters. For applications that require simultaneous detection of multiple targets, more than one LC sensor is necessary, significantly increasing the overall sensor size with no improvement to sensor detection range. Therefore, a two element sensor was developed comprised of a planar square spiral inductor and two parallel plate capacitors.

While the operating principle of the presented sensor is the same as current LC sensor technologies [10], it features multiple sensing elements (capacitors) sharing the same inductor. As a result, there are interferences among the capacitive elements and further investigations were performed to realize the new, two-element sensor design.

The electrical representation of the two element LC sensor is shown in **Figure 1**, where the inductor is responsible for coupling to a nearby antenna, receiving power and transmitting information about changes in resonant frequencies, and the capacitors are responsible for sensing parameters of interest in terms of changing capacitance values. The inductor is separated into different segments, for convenience, named L_1 , L_2 , etc., that are connected to capacitors C_1 , C_2 , etc., respectively. To remotely detect the sensor’s response, a network analyzer generates a frequency-varying electromagnetic field through the antenna to the sensor’s inductor and then monitors the change in the antenna’s impedance. This work focused on a sensor with two inductor-capacitor pairs for two-parameter monitoring. However, more inductor-capacitor pairs can be added to the circuit to form a more complex sensor capable of simultaneously measuring more than two parameters.

Prior to actual data collection, the background impedance (measurement with no sensor present) was collected so that all measurements could be subtracted from the background coil impedance to obtain the pure sensor response. **Figure 2** shows the measured resonance spectrum of the fabricated sensor. Two resonant frequencies

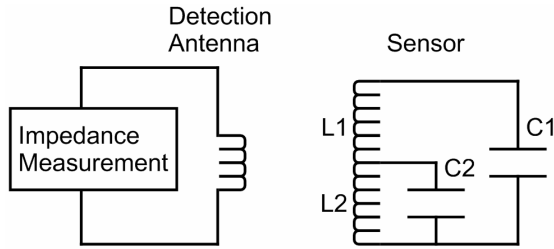


Figure 1. Circuit representation of the two-element LC sensor and the detection antenna.

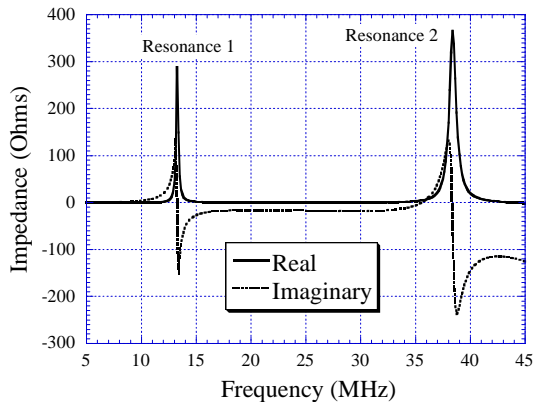


Figure 2. Resonant spectrum of the two-element LC sensor measured with the network analyzer showing two resonant peaks corresponding to C_1 (Capacitor 1) and Resonance 1, and C_2 (Capacitance 2) and Resonance 2. The values of C_1 and C_2 were both measured as 12.5 pF, and L_1 and L_2 were measured as 3.3 μ H and 4.4 μ H, respectively.

are shown on the plot, where Resonance 1 and Resonance 2 resulted primarily from C_1 and C_2 , respectively. During testing, loading C_1 caused a decrease in Resonance 1 due to an increase in the capacitance value of C_1 . However, there was also a slight decrease in Resonance 2 even though loading on C_2 remained constant. This interference is expected and explained as a result of the interdependence between capacitors physically connected to one inductive spiral (see discussion for additional details). To account for this, an algorithm was developed to determine the actual force based on the changes in both resonant frequencies.

2. Experiments

2.1. Analytical Model

An analytical model was developed to simulate the sensor response. The model was based on the equivalent circuit in **Figure 1**, assuming for simplicity that the coupling magnitudes of each inductor loop were equal at all frequencies (see **Figure 3**). Note the addition of R_1 and R_2 to more accurately predict the losses in the inductors and capacitors. The inductance, capacitance, and resistance values of the sensor were measured using an impedance analyzer (Agilent 4192) and were used for all simulations. The analytical circuit equations were plotted with MATLAB.

To determine the change in capacitance due to force loading, the compressive strain of the sensor’s parallel-plate capacitors during force loading was determined experimentally using a TestResources Inc. 100 Series mechanical testing device. The device exerted a compressive load (0 - 100 N) onto the sensor’s capacitors while measuring the compression of the capacitors. This allowed calculation of the change in the distance between the two plates of the capacitor for determination of the capacitance by the equation [11]:

$$C = \frac{\epsilon A}{d} \tag{1}$$

where ϵ is the permittivity of the medium between the capacitive plates, A is the overlapping surface area of the conducting plates, and d is the distance between them.

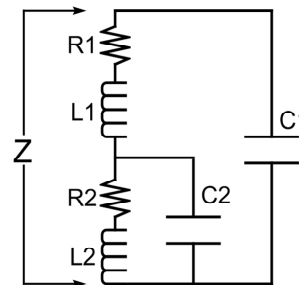


Figure 3. Circuitual model used in the MATLAB simulation.

The permittivity of the sensor medium was determined using the capacitance value, plate areas, and distance initially measured prior to loading. The capacitance calculated from change in displacement was then used as an input for the circuit model of the sensor impedance to find its resonant frequencies.

The simulation model was developed by determining the impedance of the resonant sensor, Z , when looking into the spiral inductor terminals (top of L_1 , bottom of L_2) as illustrated in **Figure 4**. The branches containing R_2 and L_2 in parallel with C_2 can be lumped as:

$$Z_2 = \frac{R_2 + j\omega L_2}{1 - \omega^2 L_2 C_2 + j\omega R_2 C_2} \quad (2)$$

where j is the imaginary number and ω is the radian frequency. Then, the series combination of Z_2 and L_1 can be

combined with the parallel C_1 , resulting in:

$$Z = \frac{j\omega L_1 + R_1 + Z_2}{1 - \omega^2 L_1 C_1 + j\omega C_1 Z_2} \quad (3)$$

Equation (3) was then evaluated in MATLAB for frequencies from 10 MHz to 50 MHz at intervals of 1 kHz to determine its resonant frequencies at capacitance values corresponding to those acquired from the force-displacement curve. The values of the electrical components used in the simulation were measured as $R_1 = R_2 = 5 \Omega$, $C_1 = C_2 = 12.5$ pF, $L_1 = 3.3 \mu\text{H}$, and $L_2 = 4.4 \mu\text{H}$. It should be noted from Equation (3) that because the poles of the resonant circuit are dependent on both capacitors, C_1 and C_2 each affect both resonant frequencies. The same analysis can be extended for additional capacitive-inductive pairs, allowing design of sensors with higher numbers of sensing parameters.

2.2. Sensor Fabrication

Figure 4 illustrates the sensor design. Sensors were fabricated from a printed circuit board using a milling machine. The line width of the pattern was 0.3 mm and the spacing between lines was 1.8 mm. The inductor part of the sensor was a square spiral measuring 90 mm \times 90 mm encompassing 10 turns. Additionally, at the center of the sensor was a rectangular conductor measuring 48 mm \times 48 mm. A parallel plate capacitor was then formed by adhering silicone foam between the conductor pad and two pieces of copper clad FR-4 fiberglass PCB, measuring 56 mm \times 27 mm each. A multiple pole LC resonant circuit was then fabricated from this setup by connecting the top PCBs to the spiral inductor. The developed sensor was monitored using a 105-mm-diameter single loop detection coil connected to an Agilent Network/Spectrum Analyzer (4396B).

To evaluate the performance of the two-element sensor in terms of signal strength, two single-element LC sensors with resonant frequencies at 10 MHz and 38 MHz, were fabricated. The single element sensor was similar in design with the previous work [10]. The lengths of the inner and outer loops of the spiral inductor of both single-element sensors were 34.4 mm and 64 mm, respectively. Additionally, the center capacitors of the single-element sensors were 32 mm \times 32 mm and the combined footprint of these two single-element sensors was equivalent to the footprint of a single two-element LC sensor. Moreover, to ensure the desired resonance was achieved (10 MHz and 38 MHz) the inductors of the sensors were adjusted to have 10 and 7 turns, respectively.

2.3. Experimental Setup and Procedure

Figure 5 illustrates the experimental setup used to evaluate the force response of the fabricated sensor. The sensor

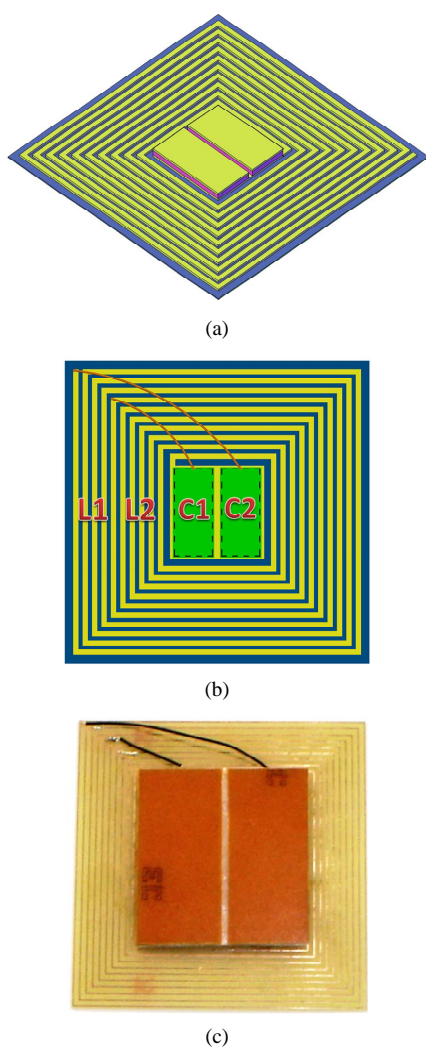


Figure 4. (a) Isometric illustration of the two-element force sensor and (b) the top view of the sensor, as well as (c) a photograph of the fabricated sensor. The wire connections between the top capacitor plates and the spiral inductor are also illustrated.

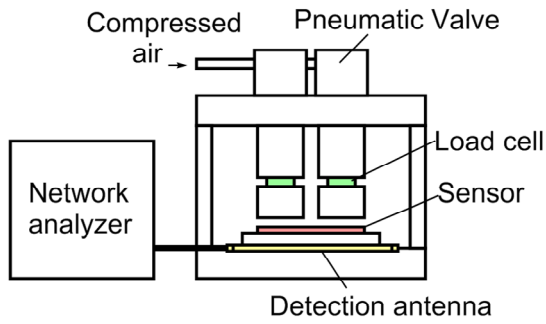


Figure 5. Experimental setup for testing the force sensitivity of the two-element LC sensor. A computer controlled pneumatic force applicator was used to apply independent force loadings on the capacitive elements of the sensor.

was placed onto a Teflon loading platform of a customized automated pneumatic mechanical loader system. The loader was controlled with a computer through standard RS232 communication using a customized Visual Basic program, and the detection antenna was situated around the loading platform. During experiments, the loader applied force to C_1 from 0 N to 89 N at 22.25 N intervals while a constant force was held on C_2 . This constant load at C_2 was then changed, from 0 N to 89 N at 22.25 N intervals, and full loading was reapplied to C_1 . The resulting sensor output was collected via an antenna with the network/spectrum analyzer. This process was then repeated with C_1 acting as the constant loading element.

To evaluate the two-element sensor against the single-element sensors, the antenna was kept stationary and connected to the network/spectrum analyzer during distance testing. The two-element sensor was adhered to a beam with double sided adhesive tape and suspended above the antenna, with the opposing end of the beam adhered to an adjustable scaffold. During characterization, the distance between the antenna and the sensor was increased at 5.0 mm intervals until the resonant peak could no longer be measured. The sensor was then returned back to its original position at 5.0 mm intervals with data being collected at each interval. This procedure was then repeated with an antenna measuring 161 mm in diameter to further characterize and compare the sensors in relation to changes in sensor response as a result of altering the antenna size. The same experiment was repeated for both single-element sensors to determine their responses against separation distance from the antenna.

2.4. Analysis Algorithm

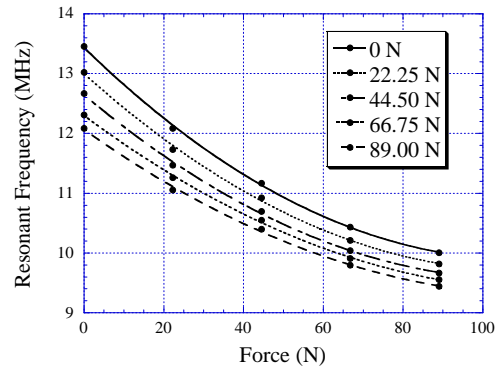
As indicated in **Figure 1**, the second LC pair (L_2 and C_2) was in series with inductor L_1 and capacitor C_1 (instead of a parallel LC pair of L_1 and C_1). As a result, the impedance of the sensor was not a simple superposition of the two LC pairs but rather a complex relationship (as

indicated in Equation (3)) that allowed the value of C_2 to interfere with the resonance of the first LC pair, and vice versa. Experimentally, the loading effect on each capacitor was also found to be interdependent on the load experienced by the other capacitor. As a result, an iterative algorithm was developed to determine the force loadings on C_1 (F_1) and C_2 (F_2) based on the resonant frequency shift of the associated resonant peaks (f_1 and f_2 respectively). Since the sensor is a forth-order circuit, the resonant frequency is expected to change with the capacitance following an inverse of quartic root curve. However, for simplicity and also due to the narrow force range, a 2nd order polynomial equation was applied to represent the resonant frequency change with loading. The 2nd order equation was found to provide a good fit with the experimental results (see **Figure 6**). Therefore, f_1 could be expressed in terms of F_1 as:

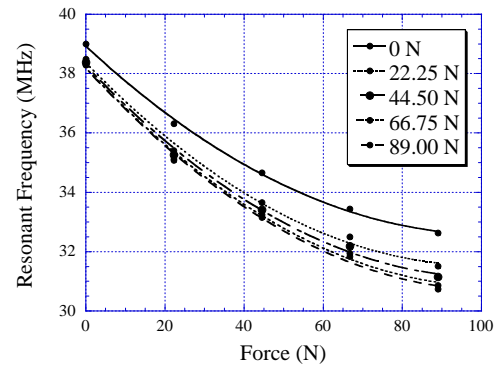
$$f_1 = A_1 F_1^2 + A_2 F_1 + A_3 \quad (4)$$

However, to accommodate the dependency of f_1 on F_2 , the coefficients in Equation (4) were expressed as:

$$A_i = a_{i1} F_2^2 + a_{i2} F_2 + a_{i3} \quad |_{i=1,2,3} \quad (5)$$



(a)



(b)

Figure 6. (a) The measured resonant frequency 1 (f_1) as a function of loading at C_1 corresponding to five different C_2 loading conditions; (b) The measured resonant frequency 2 (f_2) as a function of loading at C_2 corresponding to five different C_1 loading conditions.

where a_{i1} , a_{i2} , and a_{i3} were determined empirically. Similarly, f_2 was primarily dependent on F_2 with a slight dependence on F_1 and could thus be described by:

$$f_2 = B_1 F_2^2 + B_2 F_2 + B_3 \tag{6}$$

$$B_i = b_{i1} F_1^2 + b_{i2} F_1 + b_{i3} \Big|_{i=1,2,3} \tag{7}$$

where b_{i1} , b_{i2} , and b_{i3} were determined empirically.

The iterative process began by setting F_2 to 0 N and determining A_i using Equation (5), followed by solving for F_1 using Equation (4). The calculated F_1 was then substituted into Equation (7) to solve for B_i , which was then used to solve for F_2 with Equation (6). The value of F_2 was then substituted back into Equation (5) and the process was repeated until both F_1 and F_2 converged within an acceptable error.

3. Results and Discussion

3.1. Force Monitoring

Figure 6(a) depicts the results of loading C_1 from 0 N to 89 N at 22.25 N intervals while C_2 was held constant at 0 N, 22.25 N, 44.5 N, 66.75 N, and 89 N. The sensor was 1 cm from the center of the coil. Similarly, **Figure 6(b)** depicts the results of loading C_2 from 0 to 89 N while C_1 was held constant at different loading conditions. As can be seen, changing the constant load on the other capacitor decreased the amplitude of the force loading curve. Analyzing the changes in the curves revealed that their behavior followed a 2nd order polynomial equation. By curve fitting this data, a set of 2nd order polynomial coefficients was obtained. These coefficients were used in Equation (4) and Equation (6) to solve for F_1 and F_2 .

Figure 7 plots the calculated F_1 and F_2 when the values of f_1 and f_2 corresponding to $F_1 = F_2 = 66.75$ N were used as the input parameters for the iteration algorithm. The algorithm went through multiple iterations finding

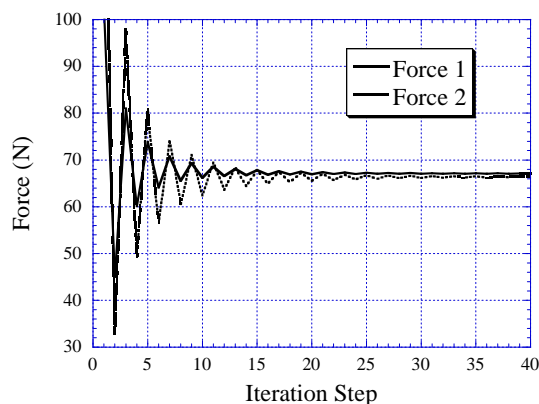


Figure 7. Calculated F_1 (force loading on Capacitor 1) and F_2 (force loading on Capacitor 2) based on the values of f_1 (resonant frequency 1) and f_2 (resonant frequency 2). The expected values for F_1 and F_2 were 66.75 N.

values for F_1 and F_2 until converging to the correct solutions. For this particular input condition, the convergence occurred at about 25 iteration steps, which was typical for all loading conditions.

Figure 8 plots the percentage errors of the calculated forces when $F_1 = F_2$. These errors were largely due to errors in the collected f_1 and f_2 data when compared to the 2nd order polynomial curve fit. Another observation in **Figure 8** is that the errors in F_2 are larger than those of F_1 . This is due to a poorer curve fitting of the dependence of f_2 on the force loading at C_1 (as indicated in **Figure 6(b)** where the curves are not as well spread as the curves in **Figure 6(a)**).

3.2. Sensor Characterization

Figure 9 shows the signal amplitudes for the two-element sensor and the two equivalent single-element sensors with increasing separation distance from the antenna. As expected, the resonant amplitudes of the sensors decreased with increasing distance between the antenna and sensor. Additionally, it can be seen that the two-element sensor had larger signal amplitude and, as a result, a larger detection range than the two single-element sensors of equivalent footprint. Moreover, the differences between the two-element and single-element sensors were also larger with the larger antenna since the coupling between the antenna and the smaller single-element sensors changed more with increasing antenna size than the coupling between the antenna and the two-element sensor.

3.3. Theoretical Validation

The result of the MATLAB simulation for the sensor impedance at zero loading is shown in **Figure 10**. As depicted, the resonant peaks are at relatively similar frequencies when compared to the experimentally measured curve from **Figure 2**. The difference of 0.2 MHz on the first resonant frequency and 0.3 MHz on the second

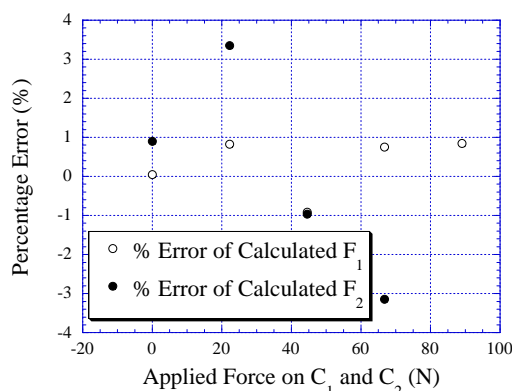
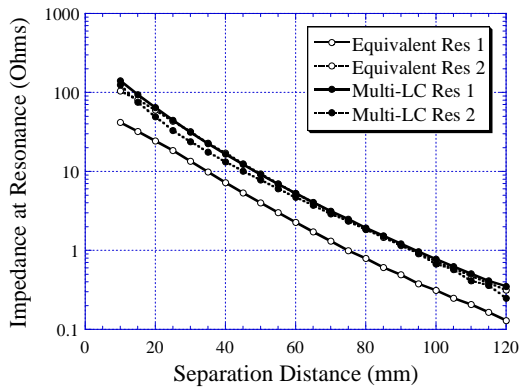
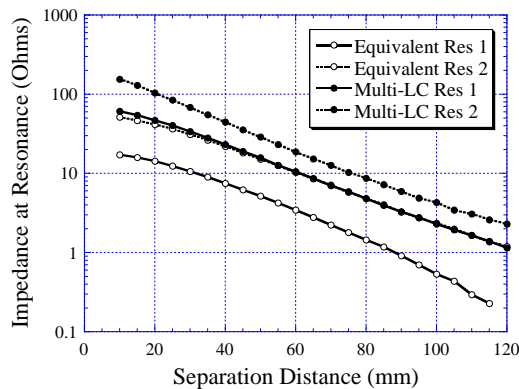


Figure 8. The percentage errors of the calculated forces compared to the actual force loadings when $F_1 = F_2$.



(a)



(b)

Figure 9. The resonant amplitudes of the two-element sensor (indicated as Multi-LC Res 1 and 2) and two single-element sensors (indicated as Equivalent Res 1 and 2) as a function of separation distance between the sensor and the antennas with diameters of (a) 105 mm and (b) 161 mm.

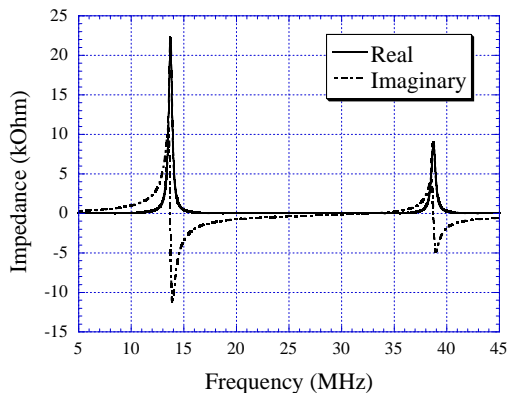


Figure 10. Simulated resonant spectrum of the two-element LC sensor showing two resonant peaks corresponding to C_1 (Capacitor 1) and Resonance 1 and C_2 (Capacitance 2) and Resonance 2. The measured sensor values were used for all simulations.

resonant frequency is due to stray inductances and parasitic capacitances not accounted for in the circuitual model.

Another notable point is the larger second resonance peak in the measurement (but not in the simulation). This

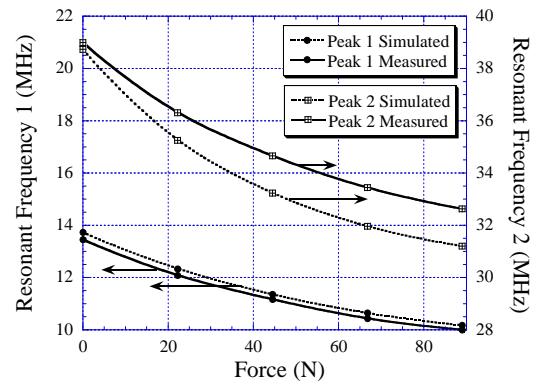


Figure 11. Comparison between simulated and measured force-frequency characteristics holding C_2 constant and measuring Peak 1 as a function of C_1 (lower two curves) and holding C_1 constant and measuring Peak 2 as a function of C_2 (top two curves).

is largely due to the self-resonance of the coil antenna (at about 60 MHz), causing signals closer to 60 MHz to be amplified. As a result, the amplification near the self-resonance of the coil antenna reflects on the measured sensor impedance.

Figure 11 depicts the simulated circuit results in correspondence to the experimentally collected data. The error between the simulated and experimental curves is likely an effect created by parasitic capacitances and inductances within the sensor circuit. In addition, the change in permittivity of the silicone foam between the capacitor plates due to compression was assumed to be negligible, but may have been significant enough to cause the observed error.

4. Conclusions

A wireless passive LC multi-element sensing array was presented. The fabricated system functioned by incorporating two parallel plate capacitors into a signal LC circuit, thus producing two resonant peaks from a single circuit. The effect of loading these capacitors was tested with a changing load of 0 N to 89 N at 22.25 N intervals applied to one capacitor while a constant load was applied to the other capacitor. The response of each capacitor was found to be interdependent on the constant load applied to the other capacitor. This interdependence was handled through the use of an iterative algorithm. A circuit model was also developed to validate the experimental results. Additionally, when compared to an equivalent setup of two single-element LC sensors, the two-element LC sensor not only had a stronger signal, and thus a larger detection range, but also exhibited less change when coupled with different sized antennas. Due to the limited detection distance (about 8 cm), the current version of sensor would be useful in places such as monitoring force loading in hard-to-reach civil engineering

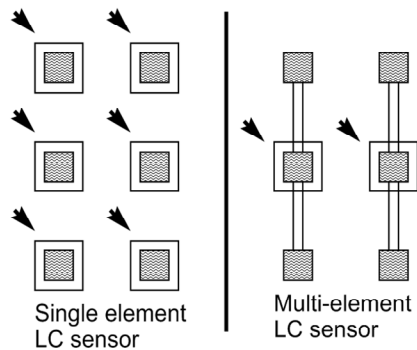


Figure 12. Illustration of the difference between single and multi element LC sensors when applying for wide area monitoring. The shaded squares represent the sensing element and the white squares the inductor. The detection points are represented by arrows.

structures, for example, concrete and wooden beams in buildings.

This device, with further development, represents an innovative method of multi-parameter/target sensing with a single LC circuit. One potential application that can highlight the advantage of this sensor compared to the previous LC sensor is as an embedded sensor for passive monitoring of stresses in a large area, such as under a roadbed. If the single-element LC sensor is employed, the user needs to monitor the response at each individual sensor location, which could be time consuming for road condition monitoring. However, for the multi-element sensor design, a number of stress-sensitive capacitor capacitors can be placed at different locations and connected to the inductor via wires as illustrated in **Figure 12**. As a result, a number of sensors can be monitored simultaneously, which can significantly shorten the monitoring time.

With further development, the number of elements could be expanded thus providing for an even more robust force mapping system. Additionally, by utilizing interdigital capacitors functionalized toward certain chemicals and environmental parameters, a sensor could theoretically be developed and deployed for monitoring multiple parameters such as humidity and volatile compounds. The future works of this system include increasing the number of elements, investigating methods to decrease overall sensor size, increasing the detection range, and adapting the system to monitor other parameters such as heat, chemical concentrations, moisture, etc.

5. Acknowledgements

The authors would like to acknowledge the National Defense Science and Engineering Grant for support of a graduate student fellow working on this project.

REFERENCES

- [1] R. A. Potyralo, T. Wortley, C. Surman, D. Monk, W. G. Morris, M. Vincent, R. Diana, V. Pizzi, J. Carter, G. Gach, S. Klensmeden and H. Ehring, "Passive Multivariable Temperature and Conductivity RFID Sensors for Single-Use Biopharmaceutical Manufacturing Components," *Biotechnology Progress*, Vol. 27, No. 3, 2011, pp. 875-884. [doi:10.1002/btpr.586](https://doi.org/10.1002/btpr.586)
- [2] C. A. Grimes, P. Stoyanov, Y. Liu, C. Tong, K. G. Ong, K. Loiselle, M. Shaw, S. A. Doherty and W. R. Seitz, "A Magnetostatic-Coupling Based Remote Query Sensor for Environmental Monitoring," *Journal of Physics D*, Vol. 32, No. 12, 1999, pp. 1329-1335. [doi:10.1088/0022-3727/32/12/308](https://doi.org/10.1088/0022-3727/32/12/308)
- [3] E. L. Tan, W. N. Ng, R. Shao, B. Pereles and K. G. Ong, "A Wireless, Passive Sensor for Quantifying Packaged Food Quality," *Sensors*, Vol. 7, No. 9, 2007, pp. 1747-1756. [doi:10.3390/s7091747](https://doi.org/10.3390/s7091747)
- [4] L. Ruiz-Garcia, L. Lunadei, P. Barreiro and I. Robla, "A Review of Wireless Sensor Technologies and Applications in Agriculture and Food Industry: State of the Art and Current Trends," *Sensors*, Vol. 9, No. 6, 2009, pp. 4728-4750. [doi:10.3390/s90604728](https://doi.org/10.3390/s90604728)
- [5] G. Stojanovic, M. Radovanovic, M. Malesev and V. Radonjanin, "Monitoring of Water Content in Building Materials Using a Wireless Passive Sensor," *Sensors*, Vol. 10, No. 5, 2010, pp. 4270-4280. [doi:10.3390/s100504270](https://doi.org/10.3390/s100504270)
- [6] C. A. Grimes, D. Kouzoudis, K. G. Ong and R. Crump, "Thin-Film Magnetoelastic Micro Sensors for Remote Query Biomedical Monitoring," *Biomedical Microdevices*, Vol. 2, No. 1, 2000, pp. 51-60. [doi:10.1023/A:1009907316867](https://doi.org/10.1023/A:1009907316867)
- [7] L. Reindl, G. Scholl, T. Ostertag, C. C. W. Ruppel, W.-E. Bulst and F. Seifert, "SAW Devices as Wireless Passive Sensors," *Proceedings of Ultrasonics Symposium*, San Antonio, 3-6 November 1996, pp. 363-367.
- [8] C. A. Grimes, C. S. Mungle, K. Zeng, M. K. Jain, W. R. Dreschel, M. Paulose and K. G. Ong, "Wireless Magnetoelastic Resonance Sensors: A Critical Review," *Sensors*, Vol. 2, No. 7, 2002, pp. 294-313. [doi:10.3390/s20700294](https://doi.org/10.3390/s20700294)
- [9] J. C. Butler, A. J. Vigliotti, F. W. Verdi and S. M. Walsh, "Wireless, Passive Resonant Circuit, Inductively Coupled, Inductive Strain Sensor," *Sensors and Actuators A*, Vol. 102, No. 1-2, 2002, pp. 61-66. [doi:10.1016/S0924-4247\(02\)00342-4](https://doi.org/10.1016/S0924-4247(02)00342-4)
- [10] K. G. Ong, C. A. Grimes, C. L. Robbins and R. S. Singh, "Design and Application of a Wireless, Passive, Resonant Circuit Environmental Monitoring Sensor," *Sensors and Actuators A*, Vol. 93, No. 1, 2001, pp. 33-43. [doi:10.1016/S0924-4247\(01\)00624-0](https://doi.org/10.1016/S0924-4247(01)00624-0)
- [11] D. Corson and P. Lorrain, "Introduction to Electromagnetic Fields and Waves," W. H. Freeman and Company, New York, 1962, pp. 58-64.